

Evolution of star forming dwarf galaxies: Characterizing the star formation scenarios

M.L. Martín-Manjón¹ *, M. Mollá,² A. I. Díaz^{1,3}, and R. Terlevich³ †

¹*Departamento de Física Teórica, Universidad Autónoma de Madrid, 28049 Cantoblanco, Madrid (Spain)*

²*Departamento de Investigación Básica, CIEMAT, Avda. Complutense 22, 28040, Madrid, (Spain)*

³*INAOE, Luis Enrique Erro 1, Tonanzintla, Puebla 72840, Mexico*

Accepted Received ; in original form

ABSTRACT

We use the self-consistent model technique developed by Martín-Manjón et al. (2008) that combines the chemical evolution with stellar population synthesis and photo-ionization codes, to study the star formation scenarios capable of reproducing the observed properties of star-forming galaxies.

The comparison of our model results with a database of HII galaxies shows that the observed spectra and colors of the present burst and the older underlying population are reproduced by models in a bursting scenario with star formation efficiency involving close to 20 per cent of the total mass of gas, and inter-burst times longer than 100 Myr, and more probably around 1 Gyr. Other modes like gasping and continuous star formation are not favored.

Key words: galaxies: evolution – galaxies: star formation –galaxies: starburst – galaxies: ISM – ISM: HII regions

1 INTRODUCTION

HII galaxies can be considered as the strong emission line subset of the Blue Compact Dwarf galaxies (BCD). Their optical emission is dominated by strong and narrow emission lines produced by the interstellar gas ionized by a young and luminous cluster. Their integrated optical spectra are indistinguishable from a normal HII region. HII galaxies are gas rich and metal poor. These facts had led to the early proposal that these systems may be very young perhaps undergoing their first burst of star formation (SF) (Sargent & Searle, 1970). However, many authors have found clear evidences of the existence of a low surface brightness, old, non-ionizing stellar population in the majority of these galaxies, as explained by Martín-Manjón et al. (2008a, here in after MMDT) and references therein. The existence of an old population plus the relative paucity of HII galaxies with extreme low metal content are consistent with a scenario in which HII galaxies are suffering at present a starburst, instead of being old systems with a slow evolution. Therefore we use the term *starburst* to denote a violent episode of star formation where a large number of massive stars have been formed in a small volume of space and over a time scale of a few million years. Galaxies called *Starbursts*

Galaxies are a very heterogeneous category, including from BCDs to ULIRGS. We will handle here only HII galaxies, those dwarf galaxies with active star formation whose effects actually dominates their UV-optical emission. In these galaxies the starburst is considered a phase, a process of strong star formation in terms of intensity and duration. Nevertheless, the fundamental details of how the star formation history proceeds in HII galaxies is still an unresolved problem.

Until now, three basic evolutionary scenarios have been postulated:

- **Bursting star formation:** the stars form in short but intense episodes separated by long quiescent periods of very low or null activity (Davies & Phillipps, 1988; Bradamante et al., 1998)
- **Gasping star formation:** The star formation takes places as long episodes of SF of moderate intensity separated by short quiescent periods (Tosi et al., 1991; Aparicio & Gallart, 1995; Recchi & Hensler, 2004).
- **Continuous star formation:** The process of stellar formation is continuous and of low intensity during the galaxy life, with superimposed sporadic bursts (Legrand, 2000).

The low metallicities, lack of dust and the optical colors argue in favour of a bursting star formation with long quiescent periods (e.g. Marconi et al., 1994). However, inactive

* E-mail: mariluz.martin@uam.es

† Research Affiliate IoA, Cambridge

star forming periods seem to rarely occur, and inter-burst stages characterized by low-levels of star formation are perhaps more plausible than its complete cessation (Lee et al., 2004). If this is the case, a continuous low level state of star formation would dominate during the vast majority of the time during which many or perhaps most of the stars in BCD galaxies would be formed.

Chemical evolution models with gasping or bursting star formation modes seem to be appropriate to describe local dwarf irregulars (dIrr) (Recchi & Hensler, 2004; Marconi et al., 1995; Tosi et al., 1991; Gallagher et al., 1996), but the chemical evidence alone cannot differentiate between gasping and bursting scenarios. The gasping scenario can be viewed as a transition between the continuous star formation and the bursting scenario (Marconi et al., 1994). The most remarkable difference between gasping and bursting scenarios is that short episodes of star formation enrich the ISM in a time scale of few tens of Myr while long-lasting episodes enrich gradually the ISM in a longer time scale, and any further episode of SF does not leave an appreciable imprint on the chemical evolution. The abundances, which increase rapidly in bursting models, change more slowly and during a longer time in gasping models, but with older ages in their stellar populations (Recchi et al., 2001, 2002). This picture, however, does not entirely exclude the possibility that star formation histories appear to be composed by burst cycles when examined with a high time resolution, but looks constant when averaged over longer time scales. It does not exclude either the possibility that the SF propagates through the galaxy, taking place in independent luminous short lived HII regions: “the short timescales associated to starbursts in dwarf galaxies may be understood as *flickering* events, small components of a larger starburst in the galaxy” (McQuinn et al., 2009)

These observations of stellar populations suggest that it is most likely that the star formation in dwarf galaxies is sporadic, separated by millions to billions of years, even in isolated systems, as most of HII are. If the SF of HII galaxies is dominated by intermittent starburst episodes separated by long inactive time spans, quiescent blue dwarf galaxies without the dominant starburst and showing similar properties to those with such intense star formation events, should be relatively common. Support to this framework comes from the fact that blue compact dwarfs (BCD), with emission lines on average much weaker than these of HII galaxies, are more common than those ones. Following this idea Sánchez Almeida et al. (2008) obtain a relationship between the duration time of the starburst phase and the quiescent periods, based on the number of objects of each type of their sample. They find that, if the duration of the burst phase is 10 Myr, the time in quiescence must be at least 0.27 Gyr, implying several mayor starburst episodes along the life of a BCD galaxy. Therefore, the diversity in properties exhibited by dwarfs may be at least partially the consequence of observing them at different times in their star formation cycles, and the frequency distributions of galaxies in the various phases could correspond to the time spent in each of them.

It would be interesting to see which is the most probable star formation scenario given by the *ab initio* cosmological hydrodynamical simulations. However this is difficult since the dwarf galaxies produced in the existing

works are usually poor gas, dwarf elliptical (dE) or dwarf spheroidals, (dSp) objects (Valcke, de Rijcke, & Dejonghe, 2008; Revaz et al., 2009; Sawala et al., 2010). Other simulations, such as Pelupessy, van der Werf, & Icke (2004) used fixed initial conditions for stellar and gas masses, and this way the mass to halo mass ratio is not a result of the simulation. In Stinson et al. (2009) simulations, the Ultraviolet (UV) background is not included, which probably contributes to a high star formation efficiency and to large final stellar masses. Mashchenko, Wadsley, & Couchman (2008) follow the evolution of a galaxy with a halo mass of $10^9 M_{\odot}$ but only until $z=5$. Governato et al. (2010) have calculated some complete hydrodynamical simulations, in which baryonic processes, as gas cooling, heating from the cosmic UV field, star formation and supernova-driven gas heating, are included with sufficient spatial resolution, with clumps as low as $10^5 M_{\odot}$ resolved. The created dwarf galaxies without bulges are similar to the observed dwarf irregular galaxies. However, besides the authors do not show the star formation histories, these galaxies show a maximum star formation rate (SFR) of $0.25 M_{\odot} \text{yr}^{-1}$ and a present SFR of $0.01 M_{\odot} \text{yr}^{-1}$, much lower than observational values for HII galaxies, and not comparable to these objects that we will try to model here. Only Nagamine (2010) has recently presented some star formation histories, obtained from cosmological hydrodynamical simulations for dwarf galaxies, with enough spatial resolution for gravitational masses of $10^9 M_{\odot}$. Their star formation histories seem to be sporadic, and the stars continue forming sporadically even at late times. However, the simulations are still having some problems to reproduce the adequate number of galaxies and the author claims that more work is still necessary. As Sawala et al. (2011) explains, all dwarf galaxies ($10^{10} M_{\odot}$) formed in the current hydrodynamical simulations are more than an order of magnitude more luminous than expected for these masses. In any case they are much more massive than BCDs and HII galaxies that we want modeling.

For what refers to other models existing in the literature, there are not models for the study of BCD or HII galaxies in the way we want to use them. A number of models have computed purely chemical evolution models for BCDs or dwarf irregular galaxies (Chiosi & Matteucci, 1982; Marconi et al., 1994; Recchi et al., 2002; Recchi et al., 2003; Shiet al., 2006; Recchi & Hensler, 2007, and many others). Most of them assume that the star formation occurs in bursts and include the effects of galactic winds and/or gas infall. However, they limit the study to the evolution of N and O abundances and/or to the luminosity-metallicity relation. Mouhcine & Contini (2002) and Vázquez et al. (2003) used the information coming from the chemical evolution models from Carigi et al. (2002) to perform the next step and combine chemical and spectral evolution for irregular galaxies. These models, however, exclude the early stages of evolution, i.e. during the nebular phase when most massive stars dominate the energy output budget. Krüger et al. (1991); Lindner, Fritze-v. Alvensleben, & Fricke (1999); Vazdekis et al. (1997) or van den Hoek et al. (2000) compute chemical and photometric evolution models in a way more or less consistent for starburst, spiral, early types or low surface brightness galaxies, respectively, any of them applied to HII galaxies. Other works, in turn, are focused on the ionized gas properties and make models

using Single Stellar Populations (SSPs) spectral energy distributions (SEDs) of a given metallicity for applying a photo-ionization code to obtain the emission lines and studying diagnostic diagrams and/or abundances obtained by empirical calibrations (Stasińska & Leitherer, 1996; Stasińska, Schaerer, & Leitherer, 2001; Stasińska & Izotov, 2003; Moy et al., 2001; Dopita et al., 2006; Martín-Manjón et al., 2010). Most of them ignore the star formation history of the galaxy and not take into account the underlying stellar population, so these studies are only valid for the study of the current stellar generations of the galaxy. Summarizing a code combining chemical, evolutionary synthesis and photo-ionization models has not been applied for the analysis of BCDs and HII galaxies, with the exception of the ours (MMDT), but only to elliptical massive galaxies (Bressan, Chiosi, & Fagotto, 1994).

The aim of this work is to critically analyze the possibility of dwarf galaxies undergo recurrent phases of star formation by comparing the predictions of our self-consistent evolutionary models with the most evolution sensitive observed parameters, i.e. stellar continuum colors, emission line equivalent widths and chemical composition in a large sample of BCD galaxies.

We have used an updated version of our models from MMDT, developed to predict the main characteristics of HII galaxies, such as the emission lines, continuum color, continuum plus the contribution of emission lines colors, equivalent widths and chemical abundances. Our code uses the chemical evolution model results for the computation of the SEDs, which are, in turn, used as the ionizing sources for a photo-ionization code. In MMDT we studied the viability of this tool, showing its adequacy in the reproduction of the data defined by the stellar populations (colors, equivalent width of absorption lines or spectral indices, spectral energy distributions...), which define the time evolution, as well as the characteristics of the gas phase (emission lines, equivalent widths, elemental abundances, gas densities), which defines the present time state of the galaxy. This is done in a self-consistent way, that is, using the same assumptions regarding stellar evolution, model stellar atmospheres and nucleosynthesis, and using a realistic age-metallicity relation.

One of the most important results obtained from our previous work was that observational data are reproduced only if the mass involved in the last burst is much smaller than the mass of the old underlying stellar population. Now, once checked the possibilities of our tool, we try to wide the number of models, changing the star formation scenarios to see if data are reproduced with more or less success for some of them.

It is a widely assumed idea that starburst galaxies are strongly affected by gas infall and outflow and that chemical abundances and star formation cannot modeled without these issues. However, the existence of outflows in dwarf starburst galaxies is by no means a settled issue; while winds able to escape the galaxy have been found in two prototypical starburst galaxies like NGC1569 and NGC1705, recent works about mass loss, for example van Eymeren et al. (2007, 2009,b, 2010), find that ionized and neutral hydrogen expansion velocities measured are, in all cases, too low to allow the gas to escape from the gravitational potential of their studied galaxies some of which, like NGC2363 or

NGC4861, can also be considered as *prototypical*. In fact, according to Bomans et al. (2007): "While the observational support for the presence of galactic winds in massive galaxies and gas-rich mergers is quite strong, the case for galactic winds in dwarf galaxies is much weaker".

The need of winds is also related with the low oxygen abundance found for dwarf galaxies for their gas fractions, and, in this case, both infall and outflow can help. However, galaxies loosing a large fraction of their gas should show red colors, contrary to what is observed. In fact, a good fraction of the galaxies in the sample of van Zee et al. (2006) can be reproduced with closed box models. Furthermore, it is necessary to take into account the N/O vs O/H relationship for dwarf galaxies. Selective winds models as Marconi et al. (1994); Bradamante et al. (1998) have recognized problems in reproducing the observed N/O ratios, and the work by Larsen, Sommer-Larsen, & Pagel (2001) demonstrates that the observed N/O ratios, as well as their dispersion, can be reproduced with closed box models while selective winds can be ruled out. Actually, Mollá et al. (2006) showed that it is mainly the combination of the different time scales in nitrogen production by stars of different masses and the galaxy star formation histories as proceeding from different star formation efficiencies, what establishes the N/O ratio.

Therefore, since there is enough proof to conclude that infall and/or outflows are not necessary to reproduce the general trends of HII galaxies, galactic supernova-driven winds are not included in our models. This scenario is also in agreement with models from Tassis, Kravtsov, & Gnedin (2008), who find that scaling relations of dwarf galaxies may be reproduced by simulated galaxies without supernova-driven outflows.

For the present work, new and updated theoretical codes have been applied for the computation of the models. The main changes correspond to the evolutionary synthesis models, now from Mollá, García-Vargas & Bressan (2009, hereinafter MGVB09) instead García-Vargas, Bressan, & Díaz (1995). As explained before, to guarantee the self-consistency of the approach we have used the same assumptions in the stellar evolution, model stellar atmospheres and nucleosynthesis parts of the code. The use of these new models allows to be more consistent than in our previous work MMDT, since there the IMF used in the chemical evolution models (Ferrini et al., 1990) and in evolutionary synthesis models (Salpeter, 1955) was not the same. The new models MGVB allow to us use the same IMF for chemical and evolutionary synthesis (photometrical) calculations. Moreover, with the previous models from García-Vargas, Bressan, & Díaz (1995) we had also a problem for the lowest metallicities stellar populations since models for the youngest ages of low metallicities were not available. Now we have models for the same number of ages for all metallicities. To include the lowest metallicities of the youngest ages change appreciably the colors of the stellar populations and allows to calculate emission lines for very low metallicity regions, as it is shown in Martín-Manjón et al. (2010). The contribution of the emission lines is quite different than expected from the simple extrapolation from other metallicities, also modifying the final results of colors.

The data shown in the graphs have been extracted mainly from two main sources. First, the compilation from

Hoyos & Díaz (2006) which provides emission line measurements, corrected for extinction, published for local HII galaxies. The sample comprises 450 objects and constitutes a large sample of local HII galaxies with good-quality spectroscopic data. The sample is rather inhomogeneous in nature, since the data proceed from different instrumental setups, observing conditions and reduction procedures, but have been analysed in a uniform way. Data for these sample objects include the emission line intensities of: [OII] $\lambda\lambda$ 3727,29 Å [OIII] $\lambda\lambda$ 4959,5007 Å and [NII] $\lambda\lambda$ 6548,84 Å all of them relative to H β , and the equivalent widths of the [OII] and [OIII] emission lines – EW([OII]) EW([OIII]) –, and the H β line, EW(H β). As a second source, we have used the metal poor galaxy data from the Data Release 3 of Sloan Digital Sky Survey, taken from Izotov et al. (2006). The Sloan Digital Sky Survey (York et al., 2000) constitutes a large data base of galaxies with well defined selection criteria and observed in a homogeneous way. The SDSS DR3 (Abazajian et al., 2005) provides spectra in the wavelength range from 3800 to 9300 Å for ~ 530000 galaxies, quasars and stars. Izotov et al. (2006) extracted ~ 2700 spectra of non-active galaxies with the [OIII] λ 4363 Å emission detected above 1σ level. This initial sample was further restricted to the objects with an observed flux in the H β emission line larger than 10^{-14} erg s $^{-1}$ cm $^{-2}$ and for which accurate abundances could be derived. They have also excluded all galaxies with both [OIII] λ 4959/H β < 0.7 and [OII] λ 3727/H β > 1.0. Applying all these selection criteria, they obtain a sample of ~ 310 SDSS objects. Data for these sample objects include the emission line intensities of: [OIII] λ 4959,5007 Å and [NII] λ 6584 relative to H β and the equivalent width of H β . They also include the intensity of the [OII] $\lambda\lambda$ 3727,29 Å emission line for the lowest redshift objects.

In the next section an explanation of the theoretical star-bursting models is made. The section 3 presents the results, the meaning of each input parameter and the implication of their variation over the results of the models. We will discuss the influence of these parameters in the reproduction of the observable characteristics of star-forming galaxies, their impact over possible star-formation scenarios and the connection among different type of dwarf galaxies in section 4. Finally, a summary and the conclusions of this work are presented in section 5. All tables of the models will be available in electronic format.

2 THEORETICAL MODELS

The viability of our model technique to reproduce the observable characteristics of HII galaxies was discussed in MMDT: In a first stage the chemical evolution model is computed by using certain input parameters to obtain the star formation history and the gas and stars chemical abundances. Secondly, the evolutionary population synthesis code is applied to obtain the SEDs corresponding to each time step of the chemical evolution. Finally, the ionizing part of the SED and the resulting abundances are used as an input to the photo-ionization code to compute the time evolution of the emission lines of the ionized gas.

2.1 Chemical evolution

The chemical evolution is computed with a simplified version of the classical *multiphase chemical evolution model* from Ferrini et al. (1994); Molla, Ferrini, & Díaz (1996); Mollá & Díaz (2005). In our version of the code there is only one region (without the two zones halo and disk)¹ with a given mass of gas which form stars (in this case we do not consider the phase of formation of molecular clouds as in the classical multiphase models). We have run models considering the star formation as a set of successive bursts followed by quiescent periods in a region with a total mass of gas of $10^8 M_\odot$. In each burst a given amount of gas is consumed to form stars, and this process comes defined by the star formation efficiency. The code solves the chemical evolution equations to obtain, in each time step, the abundances of 15 elements: H, D, ^3He , ^4He , C, ^{13}C , O, N, Ne, Mg, Si, S, Ca, Fe, and *nr* (where *nr* are the isotopes of the neutron rich elements, synthesized from ^{12}C , ^{13}C , ^{14}N and ^{16}O inside the CO core). The stellar yields are those from Woosley & Weaver (1995) for massive stars, $M > 8 M_\odot$, and those from Gavilán, Buell, & Mollá (2005) for low and intermediate mass stars. The supernova Ia yields used proceed from Iwamoto et al. (1999). The initial mass function (IMF) is taken from Ferrini et al. (1990) with a range between 0.15 and $100 M_\odot$. More recent IMFs such as Kroupa (2002) or Chabrier (2003) there exist but, for chemical evolution models, it is necessary to use a combination IMF+stellar yields sets calibrated with Milky Way Galaxy data, that is, able to reproduce the elemental abundances and gas and star densities as observed. This calibration is not still done for those IMFs, although an update of models taking these IMFs and some new stellar yield sets will be shown in a next future (Molla et al. in preparation). We have taken time steps of $\delta t \sim 0.7 \text{ Myr}^2$ from the initial time, $t = 0$, up to the final one, $t = 13.2 \text{ Gyr}$. At each time step, the star formation rate and the mass in each phase – low mass, massive stars and remnants, total mass in stars created, and mass of gas – are also obtained.

2.2 Evolutionary synthesis

The SEDs are taken from the PopStar evolutionary synthesis models by MGVB09. Isochrones are an update from those from Bressan, Granato, & Silva (1998) for 6 different metallicities: $Z = 0.0001, 0.0004, 0.004, 0.008, 0.02$ and 0.05 . The very low metallicity model of $Z = 0.0001$ had not been included before in similar works. The age coverage is from $\log t = 5.00$ to 10.30 with a variable time resolution of $\Delta(\log t) = 0.01$ in the youngest stellar ages. We have used the Ferrini IMF results (Ferrini et al., 1990) with mass limits between 0.15 and $100 M_\odot$ in order to avoid any inconsistency with the chemical evolution code, which also uses this IMF.

To calculate the SED integrated over the whole history of the galaxy, SEDs of SSPs with the corresponding metal-

¹ It implies that there is no infall of gas over a disc, as in the spiral and irregular galaxies models

² The time step is chosen to include the fastest evolutionary phases of the most massive stars

licity and age must be convolved with the star formation history (SFH):

$$L_{\lambda}(t) = \int_0^t S_{\lambda}(\tau, Z(t')) \Psi(t') dt' \quad (1)$$

where $\tau = t - t'$ is the age of the stellar population created in a time t' and S_{λ} is the SED for each SSP of age τ and metallicity Z reached in that time t' . A SED from the SSP library, S_{λ} , must be assigned to each time step according to its corresponding age and metallicity. Taking into account the SFH, $\Psi(t)$, and the age-metallicity relation, $Z(t)$, obtained from the chemical evolution model, we know the age and metallicity assigned to each time step or stellar generation. For each one of them we have chosen the SED closest in age among those available in the grid of PopStar. However, in our models the metallicity changes continuously while the available SEDs of the library are computed only for 6 possible values. Therefore, we have interpolated logarithmically between the two SSP of the same age τ and closest in metallicities to $Z(t)$ to obtain the corresponding $S_{\lambda}(\tau, Z(t'))$. The final result is the total luminosity at each wavelength λ , L_{λ} (erg.s $^{-1}$.Å $^{-1}$), corresponding to the whole stellar population, including the ionizing continuum proceeding from the last formed stellar population.

2.3 Photo-ionization calculations

To compute the photo-ionization models, we have used CLOUDY (version c06.02 Ferland et al., 1998)³. The gas is assumed to be spherically symmetric around a point source of radiation and the pressure or density in the gas is imposed by external conditions. This allows a plane-parallel geometry treatment in which the gas may be regarded as a thin shell. A closed geometry has been taken for the calculations. All the photons which escape from the illuminated face of the cloud towards the star, go on to strike the other side of the nebula, ensuring the case B of recombination and the approximation on the spot. The number of ionizing photons, $Q(H)$, striking the illuminated face of the cloud, have been calculated directly from the total resulting SED of the models.

We derive the radius of the modelled region from the mechanical energy from massive stars with strong winds (taken from MGV09), instead of using the radius required to maintain a constant density of stellar mass through the successive bursts, as we did in MMDT. Castor et al. (1975) demonstrated that an early-type star with a strong stellar wind can blow out a large cavity or *bubble* in the surrounding gas, if it is assumed to be compressed into a thin spherical shell. The wind-driven shell begins to evolve with an initial phase of free expansion followed by an adiabatic expansion phase, and then the material collapses into a thin, cold shell as a result of radiative cooling. At this stage the gas traps the ionization front and the radiative phase begins.

In this phase the ionizing photons are absorbed and the region cools via emission in the Balmer lines. In this process, the radius of the outer shock, R_s , evolves as:

$$R_s = 1.6(L_{mec}/n)^{1/5} t^{3/5} \text{ pc} \quad (2)$$

where L_{mec} is the total injected mechanical energy (SN and stellar winds) per unit time in units of 10^{36} ergs s $^{-1}$, n is the interstellar medium density in units of cm $^{-3}$, and t is the age of the shell in units of 10^4 yr. Since we use the value of the energy at each time-step, this radius represents the instantaneous size of the region obtained by adding the winds and SNe from the previous age to this age. Therefore L_{mec} is this energy divided by the time step. Then, the ionized gas is assumed to be located in a thin spherical shell at that distance R_s from the ionizing source. This approach has the advantage of eliminating the ionization parameter as a free variable in the models since now it is computed from the physical parameters of the evolving young cluster.

The ionized gas abundances are assumed to be those reached at the end of the starburst previous to the current one. Fifteen element abundances have been introduced in the photo-ionization code: He, C, N, O, Ne, Na, Mg, Al, Si, S, Ar, Ca, Fe and Ni, obtained from the chemical evolution model, except for Na, Ar and Ni which are not computed in the model and are scaled to the solar ratio (Asplund et al., 2005). The models assume that the nebula is ionization bounded and no dust has been included in the chemical evolution models neither in the photo-ionization calculations. However dust grains mixed with the ionized gas have been partially taken into account, since we have included the depletion in refractory elements (Si, Fe, CA, Si, Mg) taken from Garnett et al. (1995). The grains can affect the absorption of the *UV* photons and decrease the electronic temperature. The density has been assumed constant for simplicity and equal to 100 cm $^{-3}$, which is appropriate for modeling HII galaxies (Hägele et al., 2008) and large circumnuclear HII regions (García-Vargas et al., 1997; Díaz et al., 2007), frequently found around the nuclei of starbursts and AGNs. Although the constant density hypothesis is probably not realistic, it can be considered representative when the integrated spectrum of the nebula is analyzed.

The shape of the ionizing continuum is defined by the pair of values (ν (Ryd), $\log \nu L_{\nu}$) (Eq. 1) obtained from the ionizing spectrum given directly by the evolutionary synthesis code.

2.4 Input parameters

Taking into account the simplified version used for our chemical evolution models, the free input parameters related with the infall time-scale and the molecular cloud formation disappear. The total mass of the initial gas is within the region from the initial time. The star formation rate is zero except during the bursts. We need to define the intensity of these bursts, and the time elapsed between them.

Each model is therefore characterized by three input parameters:

- **1 - The Initial efficiency (ϵ):** It is the amount of gas consumed to form stars in the first burst of star formation, that is, $\Psi(t) = \frac{dM_s}{dt} = \epsilon M_g$

We present here models computed with 2 values of ϵ :

³ In order to maintain the consistency with MMDT, we have used the same Cloudy version for the present work. The differences between the used version and the later ones are new features and new possibilities for the modelization, however, there are not significant differences in our model results.

- (i) High efficiency models: The first burst of star formation involves 33 per cent of the total initial mass of gas ($33 \times 10^6 M_\odot$),
- (ii) Low efficiency models: The first burst of star formation involves 10 per cent of the total initial mass of gas ($10 \times 10^6 M_\odot$).

• **2 - Attenuation:** The star formation efficiency of the following bursts is attenuated in two different ways:

- (i) By a factor which changes with the number of the burst, n , according to the expression:

$$\Psi_n = \left(\frac{1}{n}\right) \cdot \Psi_0$$

This attenuation type corresponds to a soft attenuation model (hereinafter SAM).

- (ii) By a constant factor, $k^{(n-1)}$, according to the expression:

$$\Psi_n = \Psi_0 \cdot k^{(n-1)}$$

corresponding to a high attenuation model (hereinafter HAM). In this last expression k is the attenuation factor which, in this case⁴, takes values from 0 to 1. The lower the k value, the stronger the attenuation, the burst being less efficient each time; the higher the k value, the weaker the attenuation, and then the stronger the bursts. We only show models with $k = 0.65$

• **3 - Time between bursts (Δt):** Every burst takes place instantaneously and it is followed by quiet periods, whose duration can change. For this work we have taken $\Delta t = 1.3$ Gyr for the inter-burst time, that is, one burst every 1.3 Gyr as the generic case, although we will also show some models with $\Delta t = 0.1$ Gyr and $\Delta t = 0.05$ Gyr in order to compare the different results.

The models we show here are a selection of the ones calculated and described more widely in Martín-Manjón, Mollá & López-Sánchez, 2012 (in preparation). In that work, the results of 20 models are compared with data for generic and particular low mass dwarf galaxies. We have selected the most relevant of them in order to show the effects of the input parameter variation on the resulting evolutionary history of each galaxy. The input parameters of these six models are shown in Table 1.

3 RESULTS

We will show here the main results obtained with the selected models. The **efficiency** determines the initial star formation rate and the initial metallicity of the gas. We have plotted in Fig. 1 the SFR for the 6 models. The first burst is strong in all panels, while the subsequent ones are less intense due to the decrease of the available gas to form stars and the attenuation. In a) and b) the last time computed is 13 Gyr while in c) and d) the final time is around 1.3 and 0.6 Gyr respectively. In all panels we show the observational limits as dashed (green) lines. Taking these limits into

⁴ It may be higher than 1 in models with increasing efficiency; we have computed some of these models, however, their results are in clear disagreement with most observations.

Table 1. Input parameters for the theoretical models. In column 1 it is defined the type of model according to the attenuation: soft (SAM) or high attenuation (HAM); The second column gives the parameter k which defines the attenuation; column 3 is the star formation initial efficiency ϵ , and column 4 shows the time between burst Δt in Gyr.

Num. of model	Attenuation type	k	ϵ	Δt Gyr
1	SAM	–	0.10	1.30
2	SAM	–	0.33	1.30
3	HAM	0.65	0.10	1.30
4	HAM	0.65	0.33	1.30
5	HAM	0.65	0.33	0.10
6	HAM	0.65	0.33	0.05

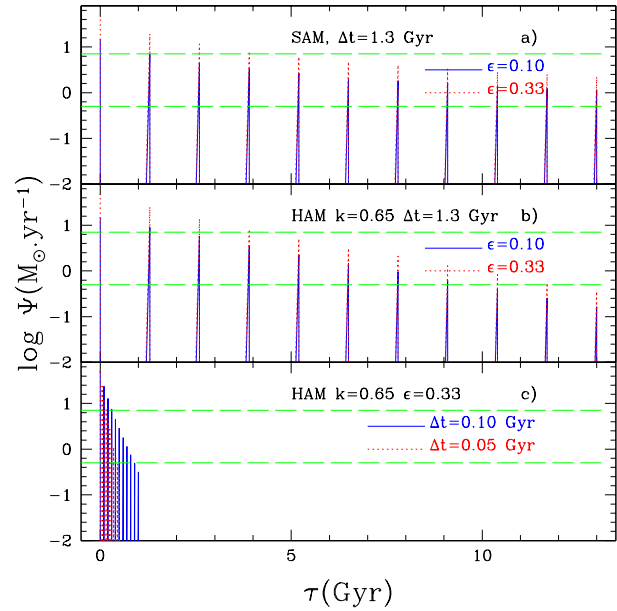


Figure 1. SFR of the models of the table 1 as labelled. In a) we show the SAM (1 and 2), in b) two HAMs (3 and 4), with the 2 same efficiencies as in a). For these 4 models the time between bursts is $\Delta t = 1.3$ Gyr. In c) we show two models (5 and 6) with shorter time between bursts, $\Delta t = 0.1$ and 0.05 Gyr. The dashed (green) lines define the upper and lower limits to the SFR estimated for BCD and/or HII galaxies by Hoyos et al. (2004).

account, the dwarf galaxies may suffer 11 bursts for SAM, or 8-9 for HAM since later bursts show rates lower than observed.

The oxygen abundances for these same models are shown in Fig. 2. In this plot we can see that the two efficiencies chosen, 33 per cent and 10 per cent, give the upper and lower limits respectively for the observed oxygen abundance range in this type of galaxies. The models with the same initial efficiency and different attenuation type, are very similar, and if Δt is shorter, the low oxygen abundance limit is reached very quickly.

Figs. 3 and 4 show diagnostic diagrams involving the ratios of intense emission lines. The number of the model (see Table 1) is given in each panel. The higher the efficiency, the more ionizing photons produced and the higher

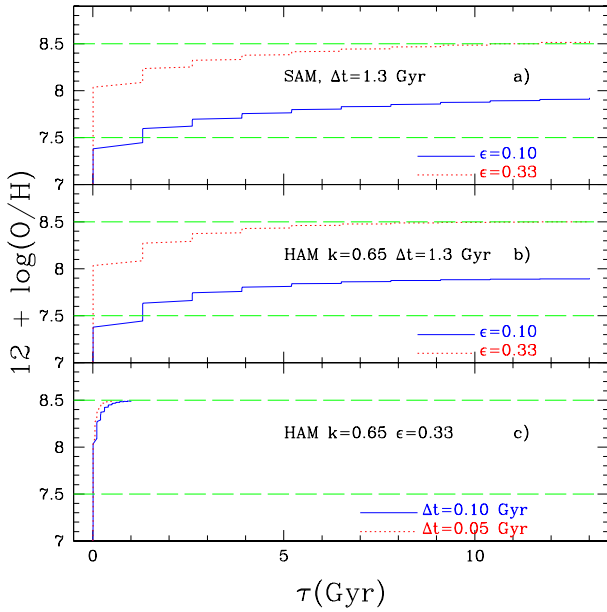


Figure 2. Evolution of oxygen abundance for same models and with the same line code as in Fig. 1. The dashed (green) lines define the observational data range

ionization parameter, leading to a higher excitation of the gas. The low efficiency models cover the region of the diagram occupied by the young and less metallic galaxies (high $[\text{OIII}]\lambda\lambda 5007, 4959/\text{H}\beta$, low $[\text{OII}]\lambda 3727/\text{H}\beta$ and low $[\text{NII}]\lambda 6584/\text{H}\alpha$), as expected. The high initial efficiency models reproduce high excitation and high abundance galaxies, with high $[\text{OIII}]\lambda\lambda 5007, 4959/\text{H}\beta$ and high $[\text{NII}]\lambda 6584/\text{H}\alpha$. The ionization degree is driven by the efficiency of the bursts, not by the attenuation mode or attenuation factor. Thus, the models with different attenuation modes and the same initial efficiency do not show noteworthy differences, since it is the current burst of star formation which produces the observed emission lines, and the underlying population does not affect the ionization parameter.

The attenuation sets the SFR of the successive bursts and determines the contribution of the underlying population. A higher attenuation implies a larger contribution of previous bursts to the total SED. Therefore, it is important to see the attenuation factor effect on the evolution of the broad-band continuum colors.

In Fig. 5 we show the evolution of the modeled continuum colors for each burst of star formation. The inclusion of nebular emission continuum in the computation of the SSPs reddens the colors of very young populations significantly, mainly at low metallicity as explained in MGVBO9.

The HAM cases, compared with SAM, have a higher contribution from the non ionizing underlying continuum, which makes the colors redder for subsequent bursts and the young and blue population features disappear. Meanwhile, SAM maintains blue colors, characteristic of the current burst of star formation.

In Fig. 6 the evolution of the colors is shown including the emission lines contribution to the wide band filters. We have done so taking into account the strongest emission lines that contribute to the color in each broad-

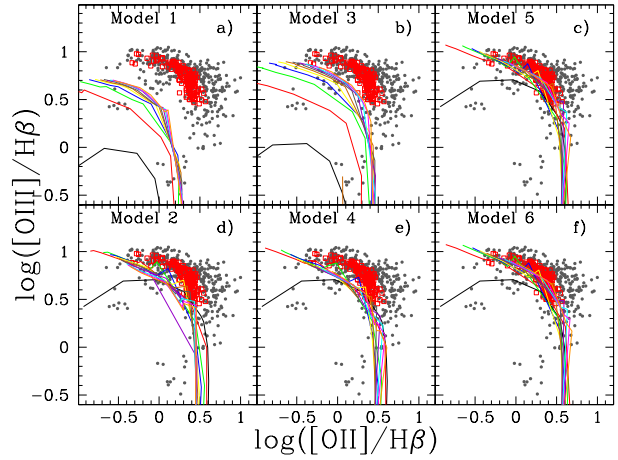


Figure 3. Diagnostic diagram for the computed models involving $[\text{OIII}]\lambda\lambda 5007, 4959/\text{H}\beta$ vs. $[\text{OII}]\lambda 3727/\text{H}\beta$ of low (top panels) and high (bottom panels) initial efficiency models corresponding to the SAM at the left and to the HAM at the right and center panels. The different colored lines represent each burst, from the first one occurred at $t=0$ Gyr (black line) to the last one at $t=13$ Gyr in models 1 to 4, at $t=1.3$ Gyr in model 5 and $t=0.6$ Gyr in model 6 (orange line). Observational data are from Hoyos & Díaz (2006) –open red squares– and Izotov et al. (2006) –grey dots–. The error of the observational data are less than 1% of the line intensity, and therefore, they are not included in the figure.

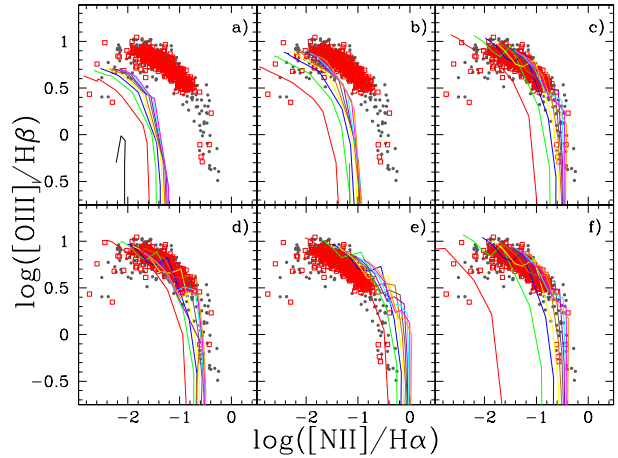


Figure 4. Diagnostic diagram for the computed models involving $[\text{OIII}]\lambda\lambda 5007, 4959/\text{H}\beta$ vs. $[\text{NII}]\lambda 6584/\text{H}\alpha$. The different colored lines and dots has the same meaning as Fig 3. The error of the observational data are less than 1% of the line intensity, and therefore, they are not included in the figure.

band spectral interval at redshift zero. These are mainly $[\text{OII}]\lambda\lambda 3727$ in U , $\text{H}\beta$ in B , $[\text{OIII}]\lambda\lambda 5007, 4959$ in V , $\text{H}\alpha$ in R and $[\text{SIII}]\lambda\lambda 9069, 9532$ in I . In that case the more intense the last burst, the larger the change in the colors, so the dotted lines are more similar to colors calculated only with the stellar populations than those shown by solid lines for higher efficiencies. On other hand, not all bands are equally modified at the same time.

A fine tuning of the attenuation factor can be obtained from the evolution of the broad-band continuum colors ver-

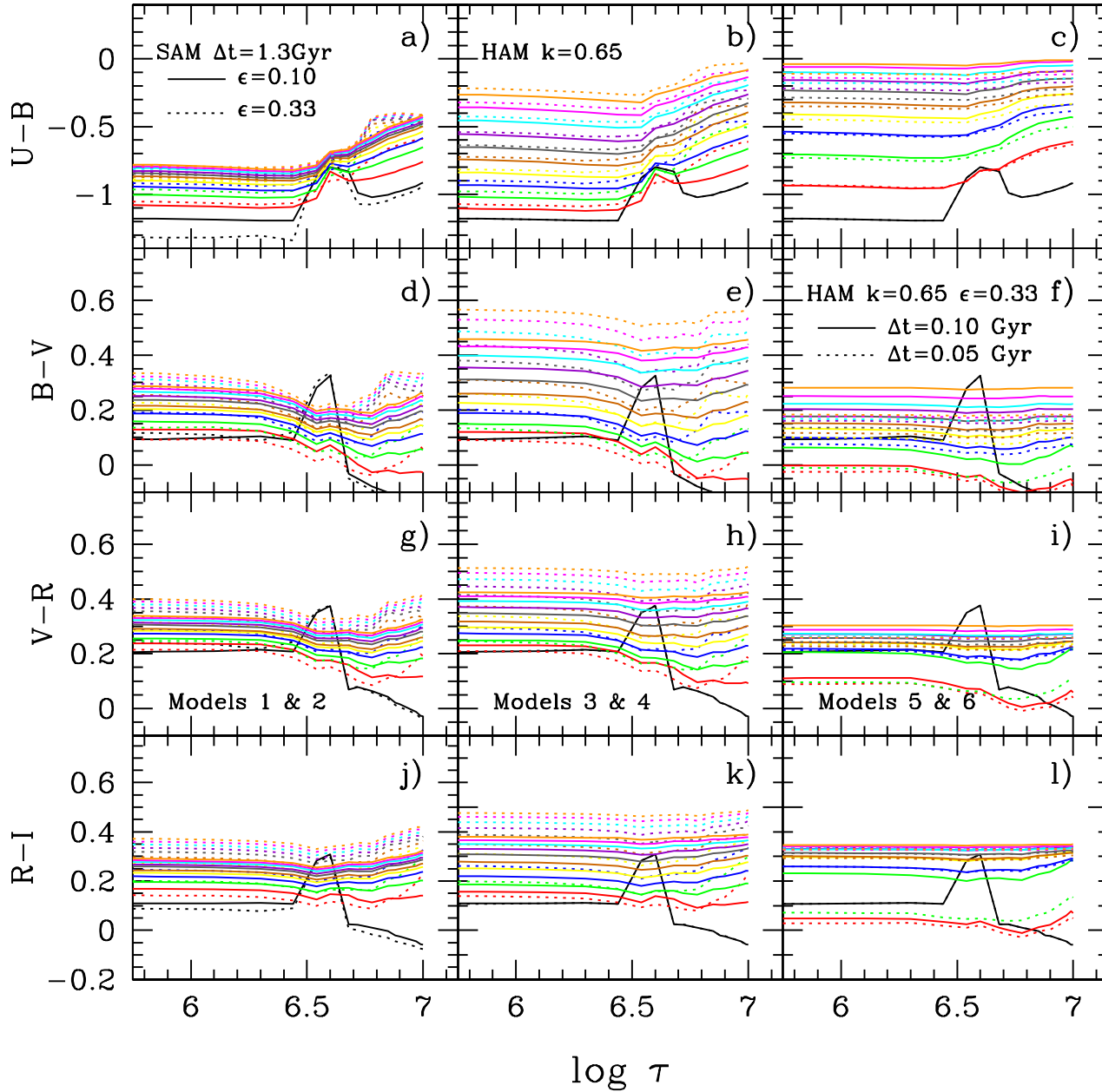


Figure 5. Evolution of the continuum colors, U-B, B-V, V-R and R-I for each burst along 10 Myr. The SAM are plotted on the left, the HAM with $\Delta t = 1.3 \text{ Gyr}$ on the intermediate panel and HAM with $\Delta t = 0.1$, and $\Delta t = 0.05 \text{ Gyr}$, respectively, on the right of the diagram. All panels include the low and the high efficiency models as dashed and solid lines, respectively, excepting for the models on the right panels, which are showing both high efficiency models with different inter-burst times, 0.1 and 0.05 Gyr as solid and dashed lines, respectively. Each burst is represented with a different colour: from the first burst (black line) to the last one (orange line).

sus the equivalent width of $H\beta$, $EW(H\beta)$. These are important observations which give also an effective method to uncover the presence of old underlying stellar populations (Terlevich et al., 2004).

The comparison of models and observations shows that in most star-forming dwarf galaxies, SSPs are unable to reproduce the reddest colors shown by the data with the lowest $EW(H\beta)$ values. In fact the observed $H\beta$ equivalent width values and colors require a large contribution

from previous stellar generations (Terlevich et al., 2004; Martín-Manjón et al., 2008a). The evolution of $EW(H\beta)$ vs. a pseudo-color of the continuum, the intensities of the adjacent continua of $[OII]\lambda 3727$ and $[OIII]\lambda 5007$ lines (similar to U-V) of our models compared with the data is shown in Figure 7. The SAM and HAM cases for $\Delta t = 1.3 \text{ Gyr}$ are plotted in the two first panels. It can be seen that to reproduce the trend of observational data, shifted to red colors at low values of $EW(H\beta)$ with respect to the SSP predictions,

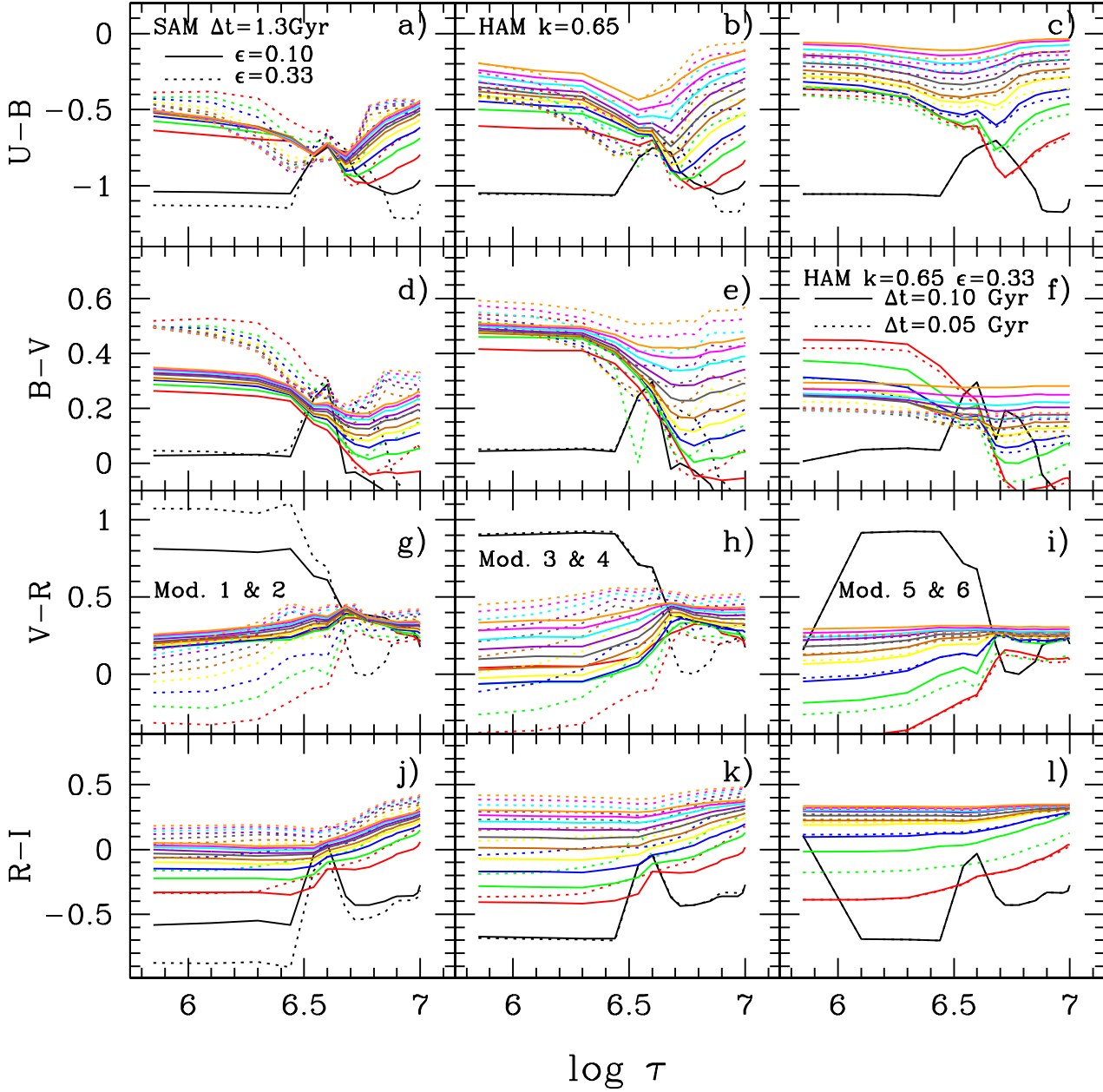


Figure 6. Evolution of the continuum colors, U-B, B-V, V-R and R-I for each burst along 10 Myr by including the contribution of the emission lines. Each model and each burst are represented with a different colour and line type similar to Figure 5.

the contribution to the total continuum of the non-ionizing red population must be much higher than the contribution of the current burst which creates the emission line spectrum. This trend can not be reproduced just with SSPs neither by increasing their metallicity or age separately nor simultaneously (MMDT). A strong attenuation in the SFR is needed, as can be seen in the center panel, to reproduce the whole range in $\text{EW}(\text{H}\beta)$ and continuum colors simultaneously.

The time between bursts (Δt) is a parameter which may also have an effect on the models similar to the attenuation. The reduction of the time between bursts offsets the

effect of increasing the attenuation: The underlying population is less evolved and produces less reddening. In Figure 7, right panel, HAM with $\Delta t = 0.1$ Gyr and $\Delta t = 0.05$ Gyr are plotted. The $\text{EW}(\text{H}\beta)$ decreases rapidly while resulting colors are not shifted to the red sufficiently to cover the range shown by the observational sample. The colors of the models with shorter inter-burst time are more similar to those with soft attenuation (strong bursts), and require an extra reddening to reproduce the needed effects of the underlying non ionizing populations. However, the $\text{EW}(\text{H}\beta)$ decreases more from burst to burst than in the case of a soft attenu-

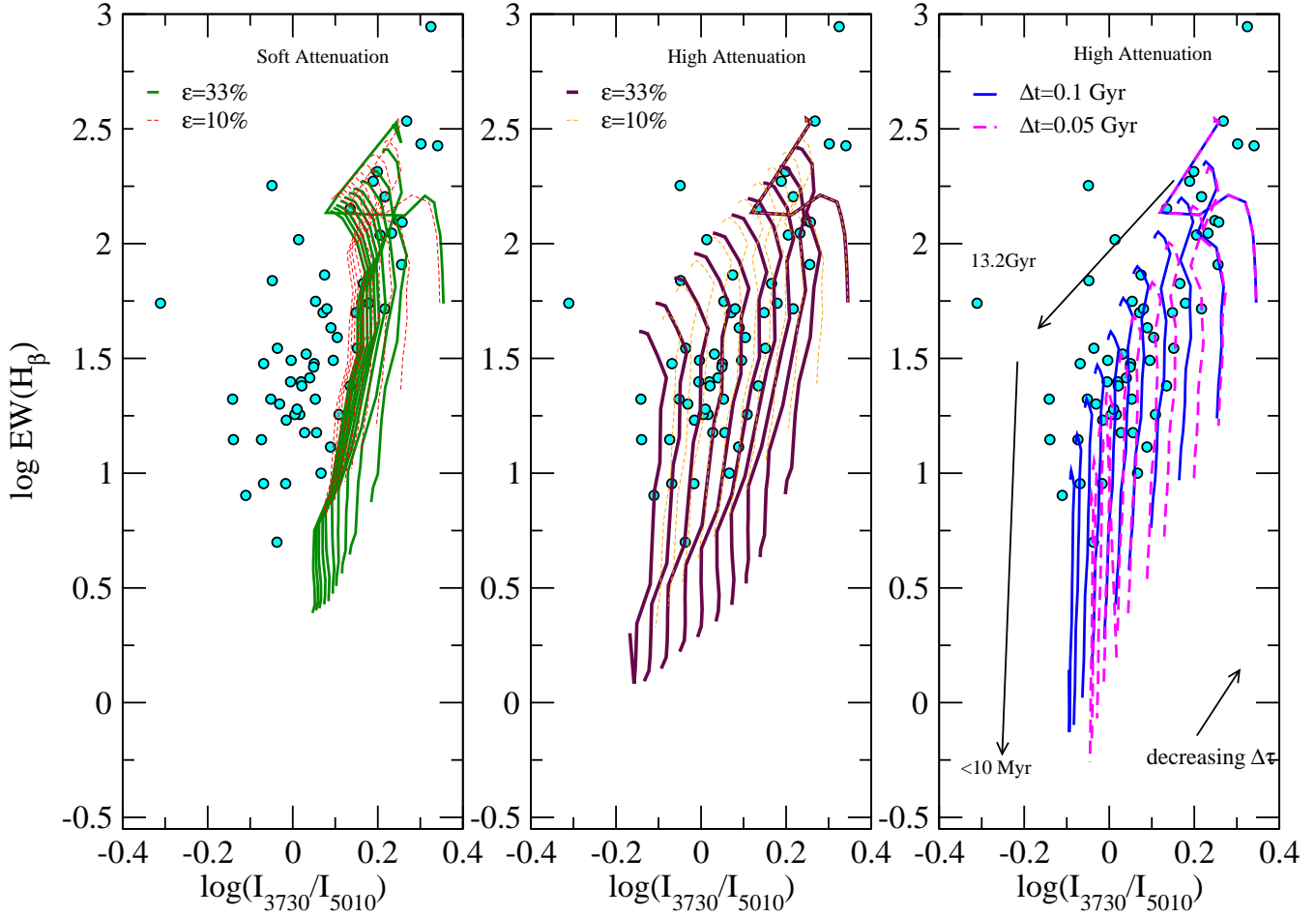


Figure 7. $\text{EW}(\text{H}\beta)$ vs. $\log(I_{3730}/I_{5010})$ compared with observational data from Hoyos & Díaz (2006), Terlevich et al. (1991) and Salzer et al. (1995), for different attenuation parameters: SAM (left panel), HAM (central panel), and including both, high and low, initial efficiencies, shown as solid and dashed lines respectively. The third panel, on the right, corresponds to high efficiency HAM with different inter-burst time, $\Delta t = 0.1$ Gyr (solid blue lines) and $\Delta t = 0.05$ Gyr (dashed magenta lines).

ation, where it maintains a high value at the beginning of every bursts. In order to reproduce the observed trend, the inter-burst time must be longer than 100 Myr.

In brief, to reproduce the observable characteristics of star-forming galaxies we have to adjust the three input parameters:

- The initial efficiency must be between 0.10 and 0.60 in order to produce a first burst which provides oxygen abundances within the observed values. In fact, efficiencies lower than 10% seems more probable to reproduce most of observations.
- Most (perhaps all) HII galaxies require the contribution of previous stellar generations to explain the observed trends shown by their continuum and emission line properties. The chemical and spectro-photometrical parameters (equivalent widths and colors) obtained by our models reproduce the observed relations if the contribution of the underlying population from previous bursts to the total continuum is higher than the contribution of the current burst of star formation which dominates the observed emission line spectrum. This implies a history of star formation higher in the past than at present, and, even in that case, attenuated burst along

the time. The fine tuning of observations is obtained by the adjusting of the attenuation factor, once the initial efficiency is fixed. (see Martín-Manjón et al. 2012 for details)

- The inter-burst time must be shorter than 1.3 Gyr and longer than 100 Myr. With shorter periods than 100 Myr the underlying continuum is too blue and its contribution to the color do not reproduce the trend shown by HII galaxies.

4 DISCUSSION

4.1 The different star formation scenarios.

Three star formation scenario are usually discussed in relation with the evolution of dwarf galaxies, (a) Burst: short star-formation episodes with large quiescent periods, (b) Gasp: long moderate star-formation episodes with short quiescent periods and (c) Continuous or almost continuous star formation with few over-imposed sporadic bursts. The three cases can be simulated by our models simply with a change of parameters:

- The star-bursting scenario (a) is this one shown in the previous sections. The effects of an instantaneous burst can

be seen in the emission lines during 10 Myr after the burst takes place. Long quiescent periods or, in our case, null star formation periods, have been considered to last more than 1 Gyr, which would be the minimum age of the underlying population belonging to the previous burst. Bursts occurred before the immediately previous one have very poor contribution to the current total continuum luminosity, and the use of this long time for the inter-burst period produces a similar result to assuming a two-burst model for some parameters, as $EW(H\beta)$. However, differences appear between both scenarios since the ISM is enriched by every single burst occurring during the galaxy life time, stellar populations older than 1 Gyr should be present, and in consequence colors would be shifted to the red.

- The gasping star formation scenario (b) can be simulated by substantially increasing the attenuation of the burst and reducing the inter-burst time. With the change in these two parameters we make a smoother and more moderate the star formation. Since the subsequent bursts are closer in time, the quiescent periods are shorter. Models with extreme attenuation and inter-burst times shorter than 100 Myr can be considered a good approximation to gasping models. This particular choice of parameters has important consequences when compared with the observations. Increasing the attenuation a major contribution to the continuum by the previous bursts is obtained. However, if, in addition, the inter-burst time is reduced, the underlying population will become younger and bluer. This approach would predict the presence of intermediate age stellar populations, younger than 1 Gyr, even after several star bursts. With larger inter-burst times only the immediately previous stellar generation contributes substantially to the present continuum, but even older stellar generations would be noticeable if we further reduce the time between bursts. Although complicated, it is also possible to simulate more extended star-burst phases by concatenation of several star-bursts. However, population synthesis modeling of BCD spectra does not favor extended periods of star formation (Mas-Hesse & Kunth, 1999). Then, if the starburst phase is short, there should be many of these episodes during the galaxy lifetime. According to Sánchez Almeida et al. (2008), there should be one BCD phase each 0.3 Gyr, which agrees with our models.

- Under a continuous star formation scenario (c), the SFR must be very low and extended. If we reduce the inter-burst time to a minimum value and, simultaneously, we reduce the intensity of each burst, we obtain a very low star formation rate, not comparable to a starburst, but similar to a continuous star formation history. In fact, many of the observable features of star-forming galaxies can be modeled with a young stellar population 3-5 Myr old and most massive stars being essentially coeval. However, as Mas-Hesse & Kunth (1999) demonstrated, it is also possible to obtain similar results with a continuous star formation, lasting at least 20 Myr since the beginning of the star formation. A low continuous star formation rate cannot be neglected, especially in low metallicity galaxies. Otherwise, if the SFR is very low, ($\log(SFR) < -3$ approximately, according to Martín-Manjón, 2009, models), there are not enough ionizing photons to produce emission lines. In this case we are not reproducing the so-called HII or BCD galaxies, but another type of galaxy or another stage of their evolution.

4.2 Connecting star-bursting models with the different evolutionary phases of a star-forming dwarf galaxy.

Actually, we may consider that, instead of a different scenario, the low and continuous star formation could be the phase occurring between bursts. In this way we could change the perspective of the problem and study the characteristics of the galaxies for the two phases: the burst and the following ~ 10 Myr, and the inter-burst, low activity periods, that is, after the first 10 Myr from the last star formation episode. In fact this is related with the two different time scales involved in the evolution, and related with different kind of data: On the one hand, a short time-scale in which the emission lines and other effects of the ionizing stellar populations are observed. On the other hand there is long time-scale which defines the red color evolution mainly due to the stellar populations older than 10 Myr.

Since a HII galaxy can be considered just a star-forming phase or a stage in the evolution of a gas rich dwarf galaxy, we can consider the inter-burst time in our models as a quiescent star-forming dwarf (QBCD) phase (Sánchez Almeida et al., 2008). Then the HII galaxy may be in the phase 10^7 yr after the star burst, in which its effects are still visible (emission lines or changes in metallicity due to massive stars ejections) and the QBCD phase would correspond to the inter-burst periods. The contribution of the young and old stellar populations in each galaxy may be obtained from the comparison of data coming from the two different time-scales, in particular, from observations as emission lines, proceeding from the ionizing stellar populations, with colors or abundances given by the older than 10 Myr stars.

As we have already seen in our previous works, MMDT and Martín-Manjón et.al (2008b), and we also show in Fig. 6, when both types of stellar populations are contributing to the light, as occurs in BCD galaxies, the colors are contaminated by the emission lines, showing in most cases different trends than those standard sequences defined by the stellar populations, either young or old. Taking into account this contamination, the colors observed are those corresponding to the ionizing continuum of a given galaxy, always during the BCD phase, that is, the colors of the young population which dominates the emitted light. In order to study the colors in the inter-burst periods and to know the properties of the underlying population, we should further eliminate the continuum arising from the starburst and isolate the properties of the underlying host galaxy.

Figures 8, 9 and 10 show the B-V vs. V-I, V-I vs. R-I and g-r vs. r-z color-color diagrams for our 6 models. Black circles show the stellar continuum colors in all panels, while the colors computed including the contribution by the strongest emission lines are shown as green and red for models 1 and 2 respectively, brown and orange for models 3 and 4, and blue and magenta for models 5 and 6. In order to represent these older phases we have also represented, as colored open squares, the colors corresponding to SSPs, as given in MGB09, for ages older than 10 Myr that is, without taking into account the youngest stellar populations phases, and metallicities from $Z=0.0001$ to 0.02. We have not computed exactly the colors of our inter-burst periods, but they must fall in this same region of the diagrams.

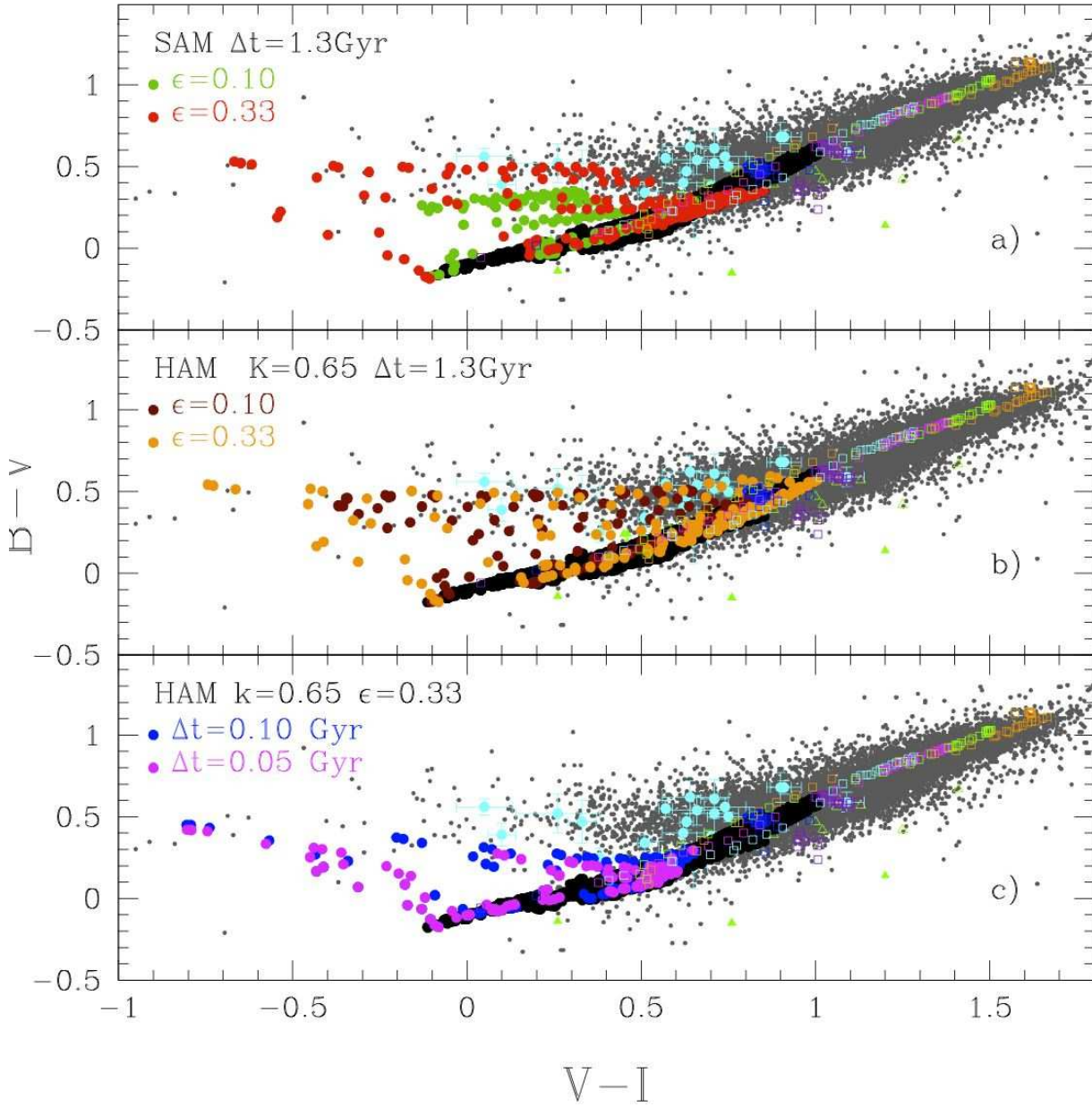


Figure 8. B-V vs. V-I color-color diagram for our models including the stellar continuum colors of the starburst phase (black dots), and these continuum colors contaminated by the emission lines. In the top panel we have green and red dots for low and high efficiency SAM models. In the middle panel, models 3 and 4 as brown and orange dots; And in bottom panel models 5 and 6 with blue and magenta dots. Colors of the inter-burst periods (age > 10 Myr) for 6 metallicities are the open (colored) squares. Observational data are taken from Sánchez Almeida et al. (2008) -grey small dots- and from Cairós et al. (2002, 2001a) -cyan full dots and green open and fill triangles (see text for an explanation).

In the B-V vs. V-I diagram (Fig. 8) the inclusion of the emission lines contribution to the continuum colors shifts the position of the model points almost perpendicularly to the originally computed ones. The location of the points is mainly determined by the contribution of strong

[OIII] $\lambda\lambda 5007, 4959$ emission lines to the V band, and, logically, they are closer to the normal stellar populations locus when efficiency is low. This means that the excursion from locus defined by the main sequence for stellar populations is stronger when the star formation efficiency is higher, lead-

ing the points far. We also show in this figure the data by Cairós et al. (2001a,b) as cyan dots with error bars. This set of observations corresponds to readily observed colors, including both continuum and line emission, and no reddening correction has been applied. It can be seen that some of the data are impossible to be reproduced by the models which do not take into account the contribution by emission lines, even if some amount of reddening is invoked. On the other hand the data by Cairós et al. (2002) of resolved locations in Mrk 370, shown in the figure as open green triangles are very well reproduced by our continuum colors. The data of Mrk 370 are based on *UBVRI* broadband and H α narrow band observations. In this case, the authors subtracted the contribution of the underlying continuum from the old stellar population, removing the contribution from emission lines and correcting for extinction, measuring in this way true colors of the young star-forming knots. This way while open green triangles correspond to the observed Mrk 370 colors, including the emission lines contribution and the underlying stellar population, the full green triangles are the stellar population colors after correction of extinction, emission lines and old stellar populations. In this case we see that some points fall out of the expected region of models which we interpret as probably due to a over-correction with SSPs models. The underlying component has colors redder than the BCD ones, and they are also well reproduced by our models.

In Fig. 9 we plot V-I vs. V-R, with the same data and code from Cairós et al. (2001a,b, 2002) and Sánchez Almeida et al. (2008) than in the previous figure. Moreover, we have also included the data of BCDs and its hosts from Telles & Terlevich (1997). This sample consists of 15 BCDs for which they observed the total colors. The data corrected of extinction are the green stars. When they correct of the emission lines effect, they obtain the colors shown by magenta stars. These points corresponding to the actual young stellar populations are closer to the region where our models are represented by the same coloured dots as in Fig. 8. They subtracted the contribution of the underlying galaxy by assuming the mean surface brightness of the extensions, or hosts, to be constant and representative of the underlying galaxy within the starburst regions. Summarizing, they give separately the colors of this underlying stellar continuum (blue stars) within the starburst, the contributions including the emission lines (green stars) and the colors of the BCD stellar continuum (magenta stars), corrected from emission lines, which are close to black dots, corresponding to our continuum BCD phase. The colors of the isolated host galaxy (blue stars) show redder colors than the BCD component, in agreement with QBCDs, Mrk 370 host and model colors with ages older than 10 Myr. Again we note some differences with our models that we assign to an over-correction of the emission lines.

Finally we represent in Fig.10 the g-r vs. r-z diagram with the same symbols that before. The selected QBCDs (Sánchez Almeida et al., 2008) are assumed to be like BCD host galaxies (Amorín et al., 2007; Amorín et al., 2009). The colors of the SSPs with ages older than 10 Myr (colored squares) can reproduce these observations, indicating that they correspond to the colors of a more evolved population than the one corresponding to the current burst in BCDs. However, some of the observed dots lie in the BCD zone,

indicating that this data sample also contains a certain proportion of BCDs, following a continuous evolutionary sequence. In this color-color diagram there is a larger difference than in the previous ones between models and data for the bluest points, showing these data higher g-r values than predicted for similar low r-z colors. Probably this is due to the transformation used to calculate SDSS colors with our Johnson colors, which would be not valid for this type of objects with emission lines contaminating the wide band filter magnitudes.

We see in the three figures that models start to separate off the main sequence of colors at different points following the type of attenuation. In the top panel, there are points with large contribution of lines starting even at the lowest and left corner, where the youngest stellar populations lie. The same points in medium panel begin to separate at redder colors, this implies that the underlying continuum corresponds to an older age. These models cover all observational range. However in the bottom panel the points with the contribution of the lines fall in a region much bluer where there are no observations. The underlying stellar populations are much younger than the populations of the data.

In any case it seems that BCDs and QBCDs colors are well reproduced by the same basic models, during the first 10 Myr after the beginning of star formation and after 10 Myr up to more than 1 Gyr respectively, and therefore we can say that both types of galaxy colors overlap and could be considered as different phases in the evolution of the same object.

5 SUMMARY AND CONCLUSIONS

Historically, the most common scenario assumed for the star formation history of the star-forming galaxies is that stars form in a bursting mode. This scenario consists in successive instantaneous star formation bursts interposed between long periods of null or very low star formation activity. If these periods are shorter and the bursts are more extended and moderate, we are under a gasping star formation scenario. On the contrary, if the star formation is low and moderate during the whole life of the galaxy, and only some sporadic bursts take place, a continuous star formation scenario is appealed.

We have analyzed the possibilities of these scenarios by means of theoretical models based on the successive bursts star formation hypothesis. Each galaxy is modeled assuming an initial amount of unprocessed gas of $10^8 M_{\odot}$. The evolution is computed along a total duration of 13.2 Gyr during which successive star-bursts take place. Since any of the possible scenarios of the star formation histories described show evidences of being able to explain the observed data, we have tried to check the hypotheses suggested.

The grid of theoretical models are computed by the combination of three tools: a chemical evolution code, an evolutionary synthesis code and a photo-ionization code, all of them previously calibrated. They have been used in a self-consistent way, *i. e.* taking the same assumptions about stellar evolution and nucleosynthesis, and the resulting metallicity in every time step. These models have three free input parameters which can be changed to obtain different model results: (a) The initial star formation efficiency which deter-

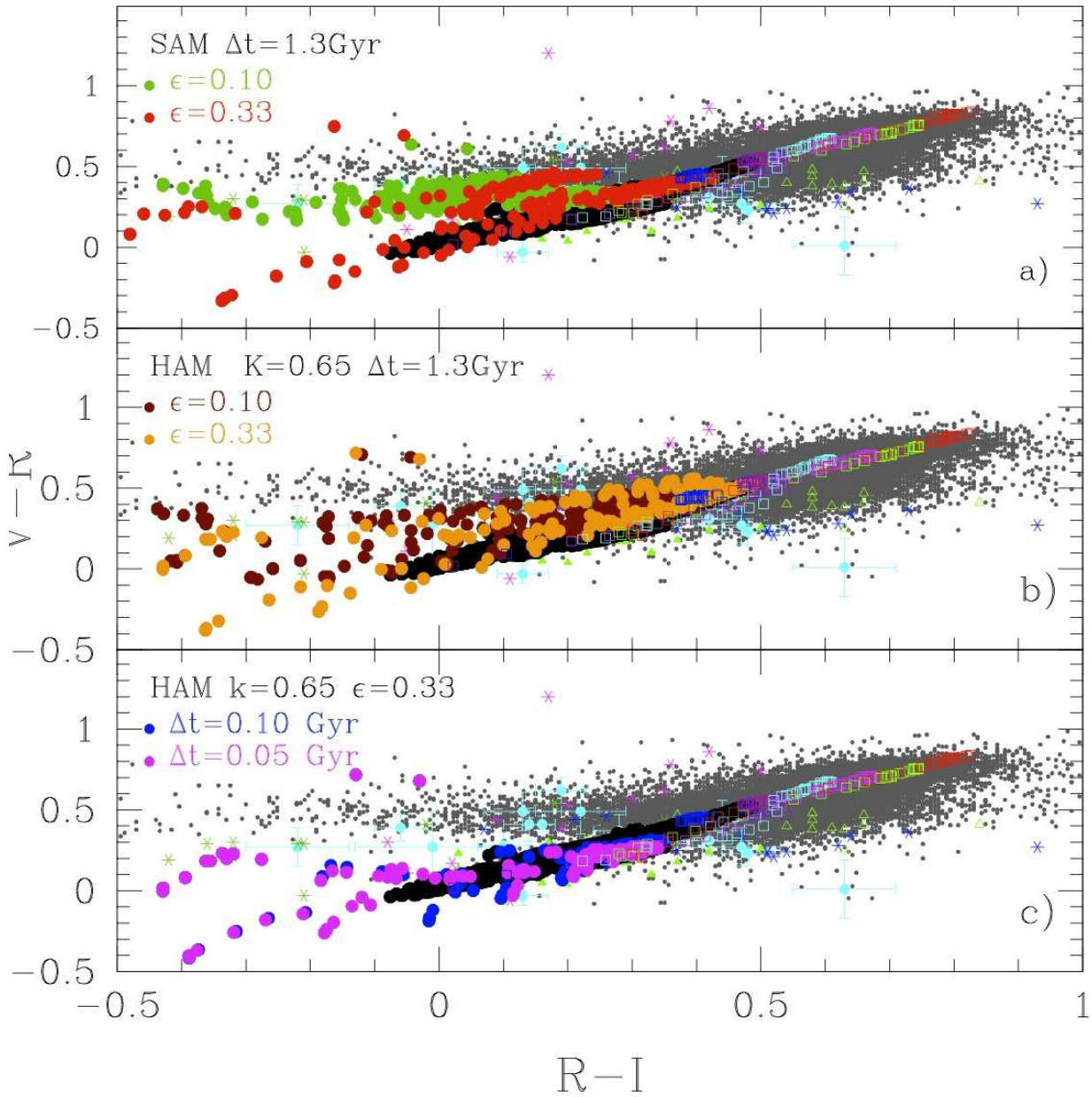


Figure 9. V-I vs. V-R color-color diagram for our models including the stellar continuum colors (black dots), and the continuum colors contaminated by the emission lines. In the top panel we have green and red dots for low and high efficiency SAM models. In the middle panel, models 3 and 4 as brown and orange dots; And in bottom panel models 5 and 6 with blue and magenta dots. Colors of the inter-burst periods (age > 10 Myr) for 6 metallicities are the open (colored) squares. Observational data are taken from Sánchez Almeida et al. (2008) -grey small dots- and from Cairós et al. (2002, 2001a) -cyan full dots and green open and fill triangles, and Telles & Terlevich (1997) -green and magenta stars- (see text for explanations).

mines the initial star formation rate (SFR) and the initial metallicity of the gas, (b) the attenuation of the successive bursts, which determines the evolution of the gas, keeping metallicity between the observational data limits, and (c)

the inter-burst time, which sets the age of the non ionizing underlying population.

We have shown that (a) also leads the behavior of the ionizing gas since emission lines are determined by the number of massive stars and the metallicity of the emitting gas.

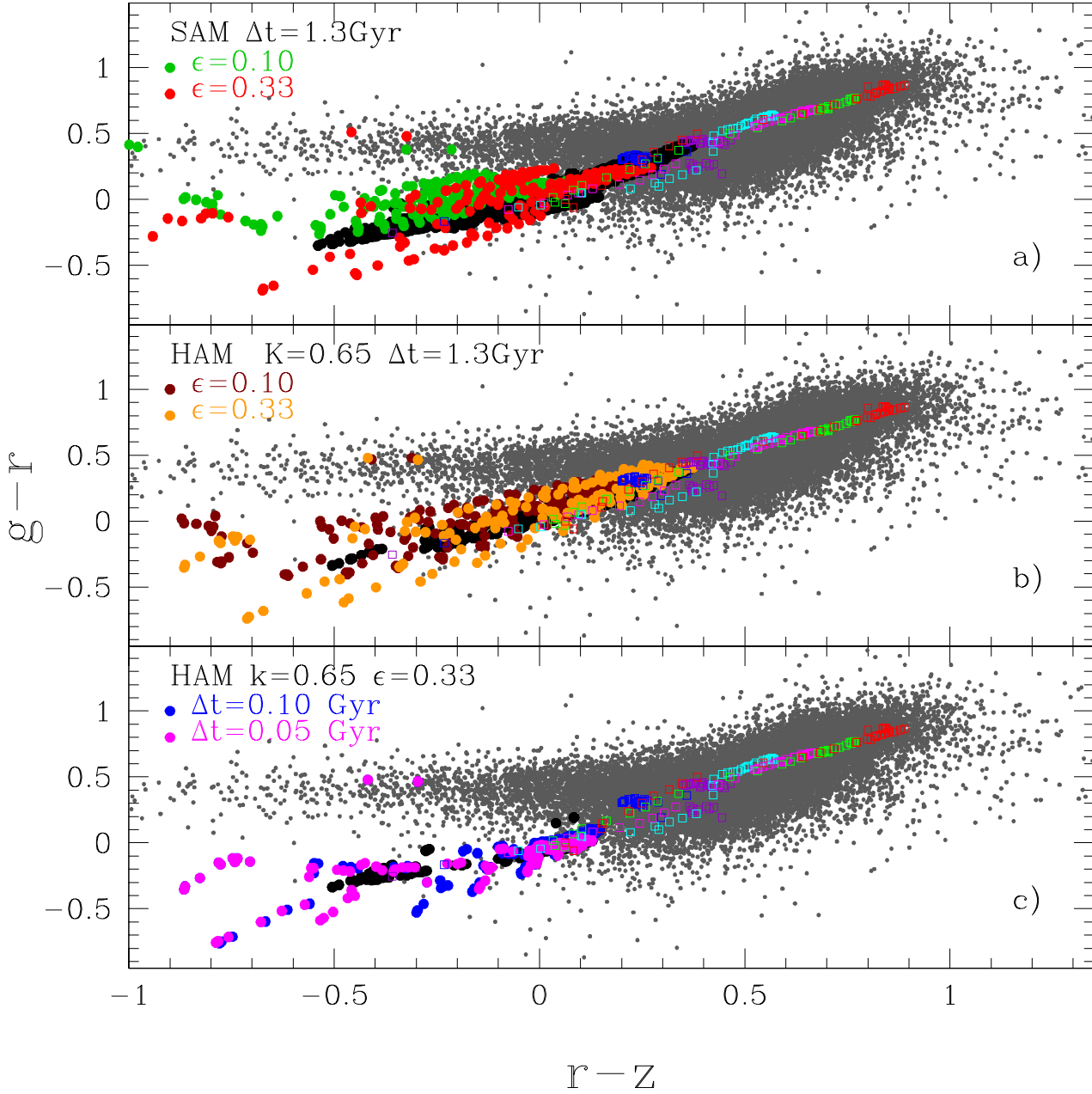


Figure 10. $g-r$ vs. $r-i$ color-color diagram for our models including the stellar continuum colors (black dots), and the continuum colors contaminated by the emission lines. In the top panel we have green and red dots for low and high efficiency SAM models. In the middle panel, models 3 and 4 as brown and orange dots; And in bottom panel models 5 and 6 with blue and magenta dots. Colors of the inter-burst periods (age > 10 Myr) for 6 metallicities are the open (colored) squares. Observational data are taken from Sánchez Almeida et al. (2008) as small grey dots

With this parameter we can control the number of old pristine stars that we are going to find in the next star formation burst.

The strength of the bursts is controlled by (b). The more attenuated, the less the star formation rate, which favors the previous stellar generations to have more weight on the total current spectrum, hence modifying the equivalent width and the colors of the continuum.

Finally, the contribution of the underlying population

can be determined by (c). These periods are the quiescent phases of the BCD. The shorter the inter-burst time, the younger the underlying stellar populations. These stars will be part of the host BCD galaxy, that is, all those generations of stars which have not ionizing stars, showing ages of more than 10^7 yr.

The models can reproduce simultaneously the data relative to the current ionizing population and the data which give us information about the evolutionary history of the

star formation. In order to reproduce the observational data, the parameters are constrained:

- a) the initial star formation efficiency must be lower than 50% and more probably is around 20% .
- b) the subsequent star-forming burst must be attenuated, in order to have the adequate proportion of underlying to young/ionizing stellar populations; and
- c) the inter-burst time must be longer than 100 Myr but shorter than 1.3 Gyr.

With our models we are able to compute the stellar continuum colors as well as the broad band colors corrected from the contribution of the more intense emission lines. This effect shifts the colors almost perpendicularly to the stellar continuum ones, specially during the first bursts of star formation, when the emission lines are more intense. The contamination of the continuum by the emission lines can make the observed galaxies appear younger than they really are, hiding evidence of underlying old populations.

On the other hand, the different characteristics shown by the star formation histories of our models, imply that we may be observing the same objects in different evolutionary stages, that is, just during the burst, in the post-burst phase or in the inter-burst periods. If we consider that the different star formation scenarios correspond to different phases in the life of a single galaxy, our models are able to reproduce the characteristics of each one of these phases. Considering the BCD phase as the first 10 Myr after a star formation burst, and the quiescent phase as the inter-burst periods, we can reproduce the galaxies both in a high activity and in a post-starburst (or pre-starburst) phase. The main difference between these phases are the existence of emission lines produced by the ionized gas. Their intensity, and their contribution to the total continuum color, can be modified by the initial efficiency. With the attenuation factor we can produce a more or less reddened stellar continuum due to the contribution of the host galaxy, the age of these old stars being determined by the inter-burst time.

6 ACKNOWLEDGMENTS

This work has been partially supported by DGICYT grants AYA2007-67965-C03-03 and AYA2010-21887-C04-02. Also, by the Comunidad de Madrid under grant S-0505/ESP/000237 (ASTROCAM) and by the Spanish MICINN under the Consolider-Ingenio 2010 Program grant CSD2006-00070: First Science with the GTC (<http://www.iac.es/consolider-ingenio-gtc>) which are acknowledged. RT is grateful to the Mexican Research Council (CONACYT) for supporting this research under grants CB-2006-49847, CB-2007-01-84746 and CB-2008-103365-F

REFERENCES

- Abazajian K., et al., 2005, *AJ*, 129, 1755
- Amorín, R. O. and Muñoz-Tuñón, C. and Aguerri, J. A. L. and Cairós, L. M. and Caon, N., 2007 *A&A*, 467, 541A
- Amorín R., Aguerri J. A. L., Muñoz-Tuñón C., Cairós L. M., 2009, *A&A*, 501, 75
- Aparicio, A. and Gallart, C., 1995 *AJ*, 110.2105A
- Asplund, M., Grevesse, N., and Sauval, A. J. 2005, in *ASP Conf. Ser. 336: Cosmic Abundances as Records of Stellar Evolution and Nucleosynthesis*, 25
- Bomans D. J., van Eymeren J., Dettmar R.-J., Weis K., Hopp U., 2007, *NewAR*, 51, 141
- Bradamante F., Matteucci F. and D’Ercole A., 1998 *A&A*, 337, 338
- Bressan A., Chiosi C., Fagotto F., 1994, *ApJS*, 94, 63
- Bressan, A., Granato, G.L., and Silva, L. 1998 *A&A*, 332, 135
- Bruzual, G. and Charlot, S., 2003 *MNRAS*, 344, 1000B
- Cairós L. M., Vílchez J. M., González Pérez J. N., Iglesias-Páramo J. and Caon N., 2001 *ApJS*, 133, 321
- Cairós L. M., Caon N., Vílchez J. M., González-Pérez J. N. and Muñoz-Tuñón C., 2001 *ApJS*, 136, 393
- Cairós L. M., Caon N., García-Lorenzo B., Vílchez J. M. and Muñoz-Tuñón C., 2002 *ApJ*, 577, 164
- Cairós L. M., García-Lorenzo B., Caon N., Vílchez J. M., Papaderos P., and Noeske K., 2003 *Ap&SS*, 284, 611
- Cairós L. M., Caon N., García-Lorenzo B., Monreal-Ibero A., Amorín R., Weilbacher P., Papaderos P., 2007, *ApJ*, 669, 251
- Carigi L., Hernandez X., Gilmore G., 2002, *MNRAS*, 334, 117
- Castor, J., McCray, R. and Weaver, R., 1975 *ApJ*, 200, L107
- Chabrier, G. 2003, *ApJL*, 586, L133
- Chiosi C., Matteucci F., 1982, *A&A*, 110, 54
- Davies, J. I. & Philipps, S. 1988, *MNRAS*, 233, 53
- Díaz A. I., Terlevich E., Castellanos M., Hägele G. F., 2007, *MNRAS*, 382, 251
- Dopita, M.A., Fischera, J. Sutherland R.S., Kewley, L.J., Leitherer, C., Tuffs, R.J., Popescu, C.C., van Breugel, W. and Groves, B.A., 2006 *ApJ Supl. Series* 167, 177
- Ferland G. J., Korista K. T., Verner D. A., Ferguson J. W., Kingdon J. B. and Verner E. M., 1998 *PASP*, 110, 761
- Ferrini F., Penco U. and Palla F., 1990 *A&A*, 231, 391
- Ferrini F., Molla M., Pardi M. C., Diaz A. I., 1994, *ApJ*, 427, 745
- Franco, J., 2003 *RMxAC*, 15, 149F
- Gallagher, J. S., Mould, J. R., de Feijter, E., Holtzman, J., Stappers, B., Watson, A., Trauger, J., Ballester, G. E., Burrows, C. J., Casertano, S., Clarke, J. T., Crisp, D., Griffiths, R. E., Hester, J. J., Hoessel, J., Krist, J., Matthews, L. D., Scowen, P. A., Stapelfeldt, K. R. and Westphal, J. A., 1996 *ApJ*, 466, 732G
- García-Vargas, M.L., Bressan, A., & Díaz, A.I. 1995 *A&AS*, 112, 13
- Gallagher, III, J. S., Hunter, D. A. and Tutukov, A. V., 1984 *ApJ*, 284, 544G
- Garnett D. R., Dufour R. J., Peimbert M., Torres-Peimbert S., Shields G. A., Skillman E. D., Terlevich E., Terlevich R. J., 1995, *ApJ*, 449, L77
- Gavilán M., Buell J. F., Mollá M., 2005, *A&A*, 432, 861
- Governato F., et al., 2010, *Natur*, 463, 203
- Hägele G. F., Díaz Á. I., Terlevich E., Terlevich R., Pérez-Montero E., Cardaci M. V., 2008, *MNRAS*, 383, 209
- Hillier, D.J. and Miller D.L. 1998 *ApJ*, 496, 407
- Hoyos C., Díaz A. I., 2006, *MNRAS*, 365, 454
- Hoyos C., Guzmán R., Bershadsky M. A., Koo D. C. and

- Díaz A. I., 2004 AJ, 128, 1541
- Iwamoto K., Brachwitz F., Nomoto K., Kishimoto N., Umeda H., Hix W. R., Thielemann F.-K., 1999, ApJS, 125, 439
- Izotov Y. I. and Thuan T. X., 2004 ApJ, 616, 781
- Izotov Y. I., Stasińska G., Meynet G., Guseva N. G. and Thuan T. X., 2006 A&A, 448, 955
- Kauffmann G., et al., 2003, MNRAS, 341, 33
- Kennicutt, Jr., R. C., 1998 ARA&A, 36, 189K
- Kewley L. J., Dopita M. A., Sutherland R. S., Heisler C. A., Trevena J., 2001, ApJ, 556, 121
- Kewley L. J., Groves B., Kauffmann G., Heckman T., 2006, MNRAS, 372, 961
- Kroupa, P., 2002, Science, 295, 82
- Krüger H., Fritze-v. Alvensleben U., Loose H.-H., Fricke K. J., 1991, A&A, 242, 343
- Larsen T. I., Sommer-Larsen J., Pagel B. E. J., 2001, MNRAS, 323, 555
- Lejeune T., Cuisinier F. and Buser R., 1997 A&A Supl.S., 125, 229
- Lee, J. C., Salzer, J. J. and Melbourne, J., 2004 ApJ, 616, 752L
- Legrand F., 2000 A&A, 354, 504
- Lindner U., Fritze-v. Alvensleben U., Fricke K. J., 1999, A&A, 341, 709
- Marconi, G., Matteucci, F. and Tosi, M., 1994 MNRAS, 270, 35
- Marconi, G. and Tosi, M. and Greggio, L. and Focardi, P., 1995 AJ, 109, 173M
- Martín-Manjón, M. L., Mollá, M., Díaz, A. I. and Terlevich, R., 2008 MNRAS, 385, 854 (MMDT)
- Martín-Manjón, M. L., Mollá, M., Díaz, A. I. and Terlevich, R., 2008 ASPC, 396, 153
- Martín-Manjón M. L., 2009, PhDT. Universidad Autónoma de Madrid, Spain.
- Martín-Manjón M. L., García-Vargas M. L., Mollá M., Díaz A. I., 2010, MNRAS, 403, 2012
- Mas-Hesse J. M. and Kunth D., 1999 A&A, 349, 765
- Mashchenko S., Wadsley J., Couchman H. M. P., 2008, Sci, 319, 174
- McQuinn, K.B.W., Skillman, E.D., Cannon, J.M., Dalcanton, J.J., Dolphin, A., Stark, D., & Weisz, D. 2009, ApJ, 695, 561
- Molla M., Ferrini F., Diaz A. I., 1996, ApJ, 466, 668
- Mollá and M., Díaz A. I., 2005 MNRAS, 358, 521
- Mollá M., Vilchez J. M., Gavilán M., Díaz A. I., 2006, MNRAS, 372, 1069
- Mollá, M., García-Vargas, M.L. & Bressan, S. 2009, MNRAS, 398, 451 (MGVB09)
- Mouhcine M., Contini T., 2002, A&A, 389, 106
- Moy E., Rocca-Volmerange B., Fioc M., 2001, A&A, 365, 347
- Nagamine K., 2010, AdAst, 2010,
- Pauldrach, A., Hoffmann, T.L., and Lennon, M. 2001 A&A, 375, 161
- Pelupessy F. I., van der Werf P. P., Icke V., 2004, A&A, 422, 55
- Recchi, S. and Hensler, G., 2004 ANS, 325, 63R
- Recchi, S., Matteucci, F. and D’Ercole, A., 2001 MNRAS, 322, 800R
- Recchi, S., Matteucci, F., D’Ercole, A. and Tosi, M., 2002 A&A, 384, 799R
- Recchi S., Matteucci F., D’Ercole A., Tosi M., 2003, Ap&SS, 284, 623
- Recchi S., Hensler G., 2007, A&A, 476, 841
- Revaz Y., et al., 2009, A&A, 501, 189
- Salpeter, E.E. 1955 ApJ, 121, 161
- Salzer J. J., Moody J. W., Rosenberg J. L., Gregory S. A. and Newberry M. V., 1995 AJ, 109, 2376
- Sánchez Almeida, J., Muñoz-Tuñón, C., Amorín, R., Aguerri, J. A., Sánchez-Janssen, R. and Tenorio-Tagle, G., 2008 ApJ, 685, 194
- Sargent W. L. W. and Searle L., 1970 ApJ, 162, L155
- Sawala T., Scannapieco C., Maio U., White S., 2010, MNRAS, 402, 1599
- Sawala T., Guo Q., Scannapieco C., Jenkins A., White S., 2011, MNRAS, 413, 659
- Shi F., Kong X., Cheng F.-Z., 2006, Chinese Journal of Astronomy and Astrophysics, 6, 641
- Smith, L., Norris, R., & Crowther, P. 2002 MNRAS, 337, 1309
- Stasińska G., Cid Fernandes R., Mateus A., Sodré L., Asari N. V., 2006, MNRAS, 371, 972
- Stasińska G., Izotov Y., 2003, A&A, 397, 71
- Stasińska G., Schaerer D., Leitherer C., 2001, A&A, 370, 1
- Stasińska G., Leitherer C., 1996, ApJS, 107, 661
- Stinson G. S., Dalcanton J. J., Quinn T., Gogarten S. M., Kaufmann T., Wadsley J., 2009, MNRAS, 395, 1455
- Tassis K., Kravtsov A. V., Gnedin N. Y., 2008, ApJ, 672, 888
- Tassis K., Kravtsov A. V., Gnedin N. Y., 2008, ApJ, 672, 888
- Telles E., Melnick J. and Terlevich R., 1997 MNRAS, 288, 78
- Telles E. and Terlevich R., 1997 MNRAS, 286, 183T
- Terlevich R., Melnick J., Masegosa J., Moles M. and Copetti M. V. F., 1991 A&ASS, 91, 285
- Terlevich R., Silich S., Rosa-González D. and Terlevich E., 2004 MNRAS, 348, 1191
- Thuan T. X. and Izotov Y. I., 2005 ApJ, 627, 739
- Tinsley, B. M., 1968 ApJ, 151, 547T
- Tolstoy E., 2003, Ap&SS, 284, 579
- Tosi, M., Greggio, L., Marconi, G. and Focardi, P., 1991 AJ, 102, 951T
- Valcke S., de Rijcke S., Dejonghe H., 2008, MNRAS, 389, 1111
- van Eymeren J., Koribalski B. S., López-Sánchez Á. R., Dettmar R.-J., Bomans D. J., 2010, MNRAS, 407, 113
- van Eymeren J., Marcelin M., Koribalski B. S., Dettmar R.-J., Bomans D. J., Gach J.-L., Balard P., 2009, A&A, 505, 105
- van Eymeren J., Marcelin M., Koribalski B., Dettmar R.-J., Bomans D. J., Gach J.-L., Balard P., 2009, A&A, 493, 511
- van Eymeren J., Bomans D. J., Weis K., Dettmar R.-J., 2007, A&A, 474, 67
- van den Hoek L. B., de Blok W. J. G., van der Hulst J. M., de Jong T., 2000, A&A, 357, 397
- van Zee, L., Haynes, M. P. and Salzer, J. J. 1997AJ, 114, 2479V
- van Zee, L., 2001 AJ, 121, 2003V
- van Zee L., Barton E. J., Skillman E. D., 2004, AJ, 128, 2797
- van Zee, L., Skillman, E. D., & Haynes, M. P. 2006, ApJ,

637, 269

Vazdekis A., Peletier R. F., Beckman J. E., Casuso E.,
1997, ApJS, 111, 203

Vázquez G. A., Carigi L., González J. J., 2003, A&A, 400,
31

Woosley S. E., Weaver T. A., 1995, ApJS, 101, 181

York D. G., et al., 2000, AJ, 120, 1579